

## Pedestal dynamics in ELMy H-mode plasmas in JET

*M.N.A. Beurskens 1), A. Alfier 2), B. Alper 1), I. Balboa 1), J. Flanagan 1), W. Fundamenski 1), E. Giovannozzi 3), M. Kempenaars 1), A. Loarte 6), E. de La Luna 4), I. Nunes 7), R. Pasqualotto 2), R. A. Pitts 6), G. Saibene 8), M. Walsh 1), and JET-EFDA contributors\**

JET-EFDA, Culham Science Centre, OX14 3DB, Abingdon, UK

1) EURATOM /UKAEA Fusion Association, Culham Sc. Centre, Abingdon, OX14 3DB, UK

2) Associazione EURATOM-ENEA sulla Fusione, Consorzio RFX Padova, Italy

3) Associazione EURATOM -ENEA sulla Fusione, C.R. Frascati, Frascati, Italy

4) Asociacion EURATOM-CIEMAT para Fusion, Madrid, Spain

5) Association EURATOM-FZ Jülich, Trilateral Euregio Cluster, D-52425 Jülich, Germany

6) ITER-IO, Cadarache 13108 Saint Paul Lez Durance, France.

7) Associazione EURATOM -IST, Lisbon

8) FUSION FOR ENERGY Joint Undertaking, 08019 Barcelona, Spain.

\*) See the Appendix of F. Romanelli et al, paper OV/1-2, this conference

e-mail contact of the main author: Marc.Beurskens@jet.uk

**Abstract:** The pedestal ELM dynamics has been studied on JET with improved diagnostic capability. The new High Resolution Thomson Scattering system enables detailed measurement of  $T_e$  and  $n_e$  pedestal profiles. A simple ELM coherent data selection technique is applied to select pre and post ELM profiles. Initial estimates using the radial profiles of ELM filaments occurring in a short time window immediately after an ELM indicate that the filaments can carry up to 30% of the ELM lost energy. On a longer time scale of 0.1-1ms after an ELM the electron density profile on JET is seen to evolve differently from the electron temperature. The temperature shows an inward collapse, whereas the density loss in the pedestal cause an increase in the SOL density which decays on a parallel transport time scale of  $L_c/c_s \sim 1$ ms. This density profile evolution is very similar for a large range of ELM sizes and plasma conditions. As a result the ELM convective losses are found to be a constant fraction of  $\sim 5$ -10% the pedestal stored energy ( $W_{ped}$ ). In baseline ELMy H-mode the conductive energy losses vary greatly with collisionality ( $\nu_e^*$ ) from  $\sim 20\%$  of  $W_{ped}$  at  $\nu_e^* < 0.1$  to  $\sim 5\%$  of  $W_{ped}$  at  $\nu_e^* > 0.5$ . In advanced tokamak (AT) scenario plasmas the collisionality is low at  $\nu_e^* \sim 0.1$  but still a large variation of the conductive ELM losses from  $\sim 5\%$  to  $\sim 20\%$  of  $W_{ped}$  is observed. The inward temperature collapse extends to  $r/a \sim 0.8$  in baseline plasmas, but varies greatly in AT plasmas from  $r/a \sim 0.5$  in unfuelled discharges to  $r/a \sim 0.8$  in lightly fuelled plasmas.

### 1 Introduction

Periodic Edge Localised Modes (ELMs) in H-mode plasmas are accompanied by an erosion of the edge pedestal due to both conductive and convective transport processes. The extent of the collapse in  $r/a$ , both in space and time, varies with ELM size and determines the energy and power load to plasma facing components. In the case of Type I ELMs in JET the fractional energy loss,  $\Delta W_{ELM}$  is almost always found to be  $> 3\%$  of the pedestal energy under standard H-mode conditions. Material studies have shown that for the wall in ITER the maximum allowed value of  $\Delta W_{ELM}$  is only approximately 1% of the ITER pedestal stored energy for the baseline  $Q_{DT} = 10$  H-mode scenario [1]. In advanced tokamak (AT) scenarios Type I ELMs pose an additional problem in that the inward propagating cold pulse following an ELM crash has the potential to affect internal transport barriers and hence can deteriorate core confinement [2-5].

The dynamics of the pedestal during the type I ELM event has been studied on JET and other devices [6-14]. Poloidally and toroidally elongated filamentary structures have been observed within  $\sim 100\mu s$  after the ELM collapse and have been observed with infrared imaging, visible cameras and divertor Langmuir probes on JET [6 and references therein]. Comparison of the observations of filaments on many devices, [7 and references therein], show that the filaments have an elliptical cross section and can carry only a small fraction of the ELM energy losses

of up to 2.5% of  $\Delta W_{\text{ELM}}$  per filament. As the toroidal model number of the filaments is  $n \sim 10$  [7], they can contain up to 25% of the ELM lost energy.

The dynamics of the density collapse  $> 100 \mu\text{s}$  after the ELM onset has been studied on DIII-D, AUG and JT-60U. Fast reflectometry measurements [8, 9,10] show that the pedestal top density collapses fast, on a time scale of  $100\text{-}200\mu\text{s}$  causing an increase in the scrape off layer (SOL) density. This change in the pedestal profile defines a pivot point around which the density profile decreases. The increased SOL density disappears on a time scale of  $< 5\text{ms}$ , much faster than the recovery time of the density pedestal. No detailed profile measurements have been available at JET until now. However, line integrated pedestal measurements from edge interferometry ( $r/a > 0.75$ ) are consistent with the observations on DIII-D, AUG and JT-60U. It was found that the density ELM-drop from interferometry lasted several milliseconds whereas the collapse in electron temperature as measured with electron cyclotron emission radiometry was faster than  $200 \mu\text{s}$ . It is likely that the timescale involved in the line-integrated density measurement on JET are related with the SOL density remaining high for several milliseconds [11].

On JET the ELM affected area as obtained from ECE pre- and post- ELM profile measurements was found to not vary much with collisionality in the baseline studies and was found to extend no further than  $r/a \sim 0.8$  as presented in [11,12]. On the contrary in AT scenario plasmas it was found that the ELM affected area can extend as far as  $r/a \sim 0.5$  [2-5]. The edge safety factor in these AT plasmas is  $q_{95} > 5$ . It remains unclear what causes the difference in ELM affected area in AT and baseline H-mode scenarios. However, the pedestal conditions are distinctly different in AT scenarios as they typically operate in a regime with high pedestal temperature and low pedestal density and high  $q_{95}$  compared to baseline plasmas. In baseline H-mode plasmas only a weak dependence of the ELM penetration depth on the edge safety factor was found, [11], and the ELM affected area reduced with increasing  $q_{95}$  from 3 to 4, indicating an opposite trend than found in the comparison between AT and baseline plasmas

It has been found on various devices [10-15] that the ELM losses in ELMy H-mode plasmas scale with the electron collisionality  $\nu_e^*$ . The ELM energy losses normalised to the pedestal stored energy ( $\Delta W_{\text{ELM}}/W_{\text{ped}}$ ) decrease for increasing  $\nu_e^*$ . The ratio of convective versus conductive losses could until this paper not be established in JET as no sufficiently spatially and temporally resolved density profiles were available. However the trends in convective versus conductive losses were compared using line integrated interferometry  $n_e$  measurements and ECE pedestal top measurements. The  $\Delta n_e/n_e$  did not vary and  $\Delta T_e/T_e$  was strongly reduced with increasing  $\nu_e^*$  [11,12]. This strong negative dependence of conductive ELM losses with collisionality was confirmed on JT60-U, DIII-D and MAST using kinetic profile measurement [10,13,15].

This paper extends the study of type I ELM profile dynamics and energy losses on JET as diagnostics capabilities have improved. Especially the availability of a High Resolution Thomson Scattering (HRTS) system enables detailed profiles studies. First an overview will be given of the pedestal conditions of the baseline and AT plasma scenarios studied. Then the analysis technique of ELM coherent averaging is explained. The ELM energy losses as obtained from the kinetic profiles are separately discussed for the filamentary phase and the slower collapse phase respectively  $< 100\mu\text{s}$  and  $> 100\mu\text{s}$  after the  $D_\alpha$  onset. A qualitative overview of the ELM dynamics in density and temperature profiles from HRTS is shown followed by a quantitative analysis of the conductive versus the convective ELM losses exploiting the AT versus Baseline data base that has been built.

## 2 Pedestal parameters in baseline and AT Plasmas

An overview of pedestal average  $n_e$  and  $T_e$  for a subset of both baseline and AT scenarios for the JET 2008 campaign is given in Figure 1. The pedestal  $T_e$  values are derived from ECE radiometry at the pedestal top and the pedestal  $n_e$  values from a vertical edge channel of the JET interferometer covering the region  $r/a > 0.75$ . A clear distinction can be seen in population of the  $n_e$ - $T_e$  diagram; the AT scenarios (1.2MA and 1.7MA,  $q_{95}=5$ ,  $\delta\sim 0.35$ ) have higher pedestal temperatures and lower pedestal densities and markedly larger pedestal  $\beta_{pol}$  than the baseline scenarios. The highest pedestal densities are seen in the high triangularity (2.5MA,  $q_{95}=3.6$ ,  $\delta\sim 0.4$ ) baseline discharges, and the low triangularity discharges populate the middle range of the  $n_e$ - $T_e$  space. A large range of plasma currents ( $I_p$ ) was obtained in the low triangularity discharges (1MA-3.8MA,  $q_{95}=3$  and 3.6,  $\delta\sim 0.25$ ), which enables to study the pedestal dynamics over a large range of  $I_p$ .

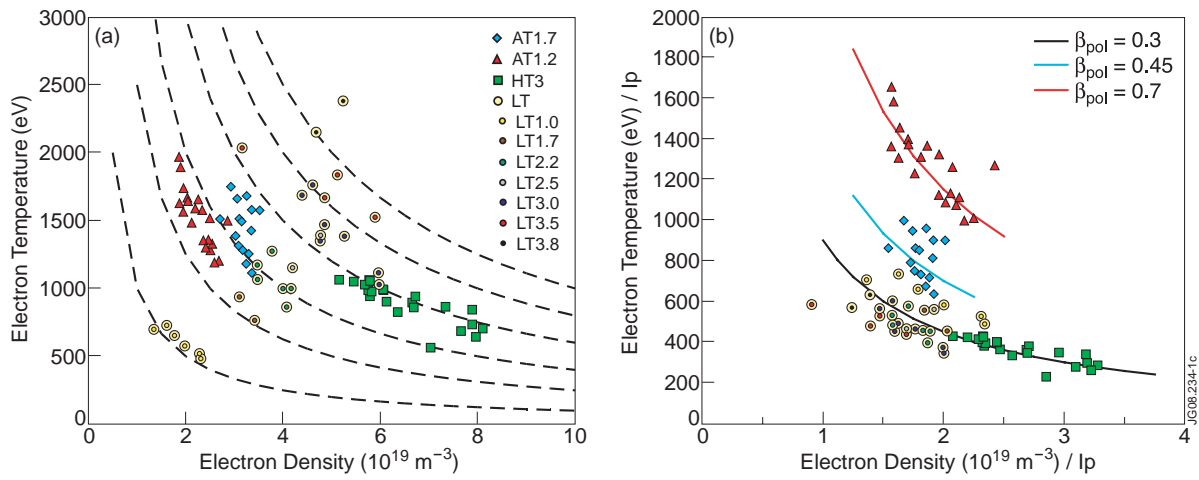


Figure 1: (a) Pedestal  $T_e$  and  $n_e$  diagram and (b) Pedestal  $T_e/I_p$  and  $n_e/I_p$  diagram to show the difference in  $\beta_{pol}$  between the AT and baseline scenarios. Red triangles and cyan diamonds are AT scenario plasmas at respectively 1.2 and 1.7MA ( $q_{95}=5$ ,  $\delta\sim 0.35$ ). Yellow circles are low triangularity ELMy H-modes (1MA-3.8MA,  $q_{95}=3$  and 3.6,  $\delta\sim 0.25$ ) and green squares represent high triangularity ELMy H-modes (2.5MA,  $q_{95}=3.6$ ,  $\delta\sim 0.4$ ).

## 3 ELM coherent data selection

In order to understand the mechanisms that cause the loss and recovery processes during an ELM cycle a detailed study of the dynamics of the JET edge pedestal is required. The system extensively used in this paper is the new HRTS system for both  $T_e$  and  $n_e$  profile measurements with 1.5cm resolution, 20Hz repetition rate and 10ns time resolution [16]. The ELM timing is obtained by identifying the spikes of the inner divertor  $D_\alpha$  spectrometer signal in JET. This gives a reference in the ELM detection of better than 100 $\mu$ s. Diagnostic data can then subsequently be sorted with respect to the onset time of the nearest  $D_\alpha$  peak. Figure 2 give an example pedestal profile reconstruction obtained using this ELM coherent data sorting. In this example the spatial coverage has been improved by a slow radial plasma movement of 1.5 cm in a 3s period. This discharge had very regular 30Hz ELMs, in which case good profile reconstruction is possible. Figure 3 shows the ELM selection applied for this shot to scalar parameters of the pedestal top  $T_e$  from ECE (0.2 ms resolution), line integrated pedestal  $n_e$  from interferometry (0.8 ms time resolution), and diamagnetic energy loss from magnetics (100 $\mu$ s time resolution). Note the different time scales of the electron density and temperature drop. This will be addressed in section 5.

#### 4 Fast Dynamics; radial profile of ELM filaments

ELM filaments have been observed on JET [6] and many other devices [15 and references therein]. They have recently also been detected in the scrape-off layer (SOL) with the new JET HRTS system on the  $T_e$  and  $n_e$  profiles after an ELM, together with strong oscillations in the edge interferometry signal and the occurrence of helical 20 cm wide stripes on the JET wall observed with a main chamber viewing IR camera [6]. The time resolved interferometry combined with edge rotation measurements indicate that the filaments have a toroidal mode number of  $n \sim 10$  (indicating the presence of  $\sim 10$  filaments). Up to 20-30 filament footprints have been observed on the main chamber wall [6], which is interpreted as a breaking up of the filaments towards the machine wall, but just outside the last closed flux surface  $\sim 10$  filaments are expected. So-far only a limited number of filament radial profile measurements have been obtained as they only occur in a very narrow time window after an ELM. However, an approximate radial extent of the filament of  $\sim 5$ cm may be seen directly in Figure 3. A rough estimate of the filament energy content can be obtained by assuming a  $5 \times 20$  cm elliptical cross-section and taking the filament length as  $2\pi R q_{95} \sim 50$ m, ( $R$  the major radius,  $q_{95} = 3$ , for the discharge in Figure 3). This yields an electron energy content of  $\sim 1$ kJ, compared with  $\Delta W_{\text{ELM}} \sim 100$  kJ for the ELM in Figure 3. No direct measurements of the ion temperature is available in ELM filaments on JET. Taking into account that ion conduction is slower than the electron heat conduction, it could be assumed that  $T_i = 2T_e$  [17]. The energy content of a single filament could then be 3 kJ. Assuming that 10 such filaments occur after an ELM event ( $n \sim 10$ ) the total filament energy could be  $\sim 30$ kJ, i.e. 30% of  $\Delta W_{\text{ELM}}$ . This is in agreement with model calculations as shown in [17]. This also represents an upper limit to the energy which could be convected to the main chamber wall surfaces since much will be dissipated along field lines by parallel transport as the filament propagates radially in the SOL. This is consistent with the smaller energy fractions of 5-10% of  $\Delta W_{\text{ELM}}$  that have been directly measured on the main walls for similar ELM sizes [17, 18]. From these observations it is clear that the filaments most likely do not carry all the energy and particles expelled by an ELM collapse, as was also found for filament measurements in MAST [7].

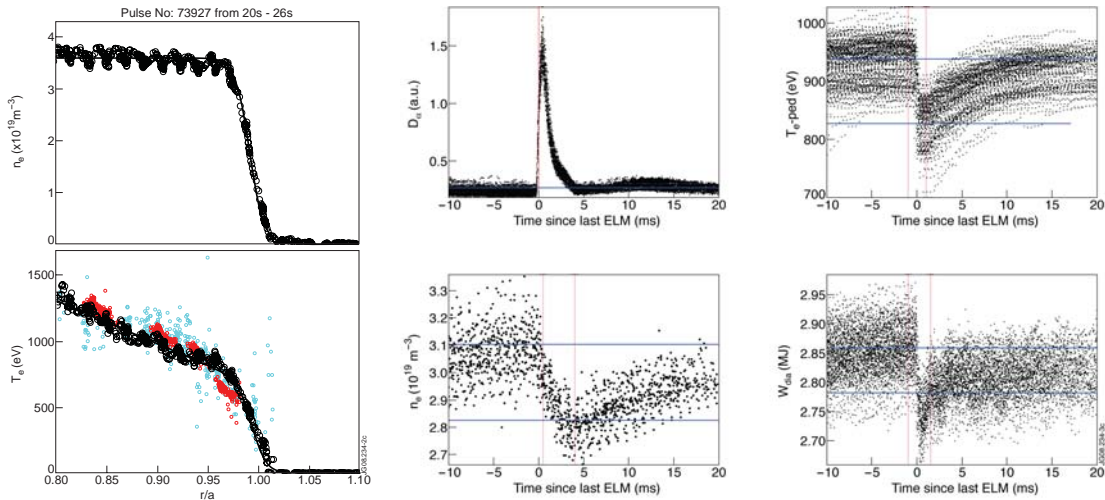


Figure 2: HRTS Profiles of  $T_e$  and  $n_e$  (black) and edge (cyan) and core  $T_i$  (red) from charge exchange diagnostics. These are ELM selected profiles in the last 3 ms before selected ELMs.

Figure 3: Example of ELM coherent data sorting for the  $D_\alpha$  signal itself, the pedestal electron temperature measurements by ECE, the pedestal electron density by Interferometry and fast diamagnetic-energy-measurements for JET pulse 73927 ( $I_p = 1.7$ MA,  $B_t = 1.8$ T,  $PNBI = 8$ MW). The onset of the ELM is at  $t = 0$  s. The blue horizontal lines show the average value just before and after an ELM crash.

## 5 Pedestal dynamics

While part of the energy contained by the filaments will reach the main chamber plasma facing surfaces, most of the remaining ELM energy release will end up on the divertor targets. The timescale of the type I ELM collapse is  $\sim 200\text{--}300\mu\text{s}$  as measured with fast ECE and fast magnetics with a time resolution of better than  $4\mu\text{s}$  [11]. As discussed in [11] a difference was found between this time scale and the duration of the collapse as seen by line integrated interferometry measurements. With the availability of HRTS profile measurements, the local dynamics of the ELM density crash can be studied using the ELM data selection algorithm. The shape of a typical type I ELM crash is shown in Figure 5 and is similar with fast profile measurements in [8, 9, 10]. The pre and post ELM profiles show that the density collapse on a millisecond time scale is quite different from the temperature collapse. The post ELM selected HRTS measurements between 0.1 and 1 ms after an ELM-onset show that the inward density profile collapse provokes a rise in the density just outside the separatrix (Figure 5a), whereas the  $T_e$ -collapse is solely downwards and inside the separatrix (Figure 5b). The HRTS profile taken on a longer timescale  $> 1\text{ms}$  after an ELM (no figure presented) show the density in the scrape off layer (SOL) has disappeared, whereas the pedestal density and temperature are still recovering from the collapse. The measured SOL density transport time scale of an order of a millisecond is compared to the time scale involving the connection length  $L_c = 2\pi R q_{95}$  and the ion sound speed  $c_{s,i} = \sqrt{2T/m_i}$ . A SOL temperature of 10-30eV leads to a typical time scale in the order of  $L_c/c_{s,i} \sim 1\text{ms}$ , in agreement with the observations.

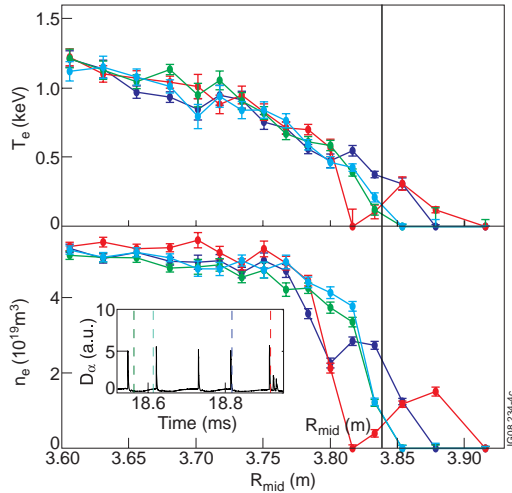


Figure 4: Observation of ELM filaments in a type I ELM H-mode. The Cyan and green profile are taken just before ( $-5\text{ms}$ ) and well after ( $20\text{ms}$ ) an ELM and represent the unperturbed profiles. The Blue and red profile are  $< 100\mu\text{s}$  after a  $D_\alpha$  ELM signature and show radial extensions of the profile, which are associated with filaments. The estimates in the text are taken from the red profile.

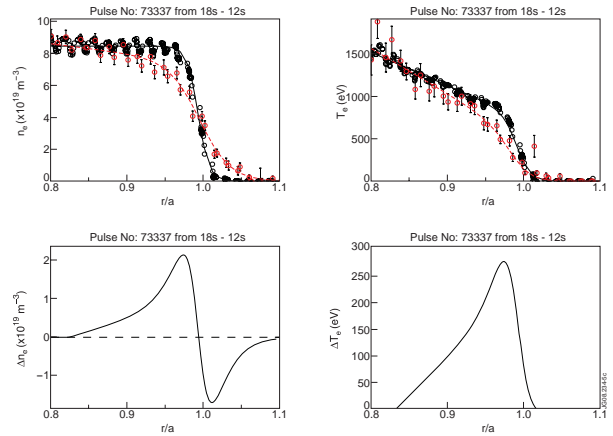


Figure 5: (a) and (b) Pre-ELM (black) and Post-ELM (red) Density and Temperature profiles from HRTS of a high triangularity ELM H-mode. (c) and (d) Particle and temperature loss due to the ELM event. Pre-ELM profiles selected in  $-1\text{ms} < t_{\text{elm}} < 0\text{ms}$  and post ELM profiles selected between  $0.1\text{ms} < t_{\text{elm}} < 1\text{ms}$ .

Figure 5 shows that the ELM affected area extends to  $r/a \sim 0.85$ . This is typical for type I ELM H-modes in JET as has been reported in [12], and is rather independent of plasma fuelling,  $q_{95}$  or heating schemes. However, in JET plasmas relevant for ITER steady state operation, with  $q_{95} = 5$  and optimised magnetic shear, ELMs are found to affect a large region of  $r/a > 0.5$  [2,3,5]. Especially for plasmas with Internal Transport Barriers (ITB) this is

worrying as the deeply penetrating Type I ELMs can deteriorate the core confinement. An example of a profile collapse in an AT plasma is given in Figure 6a. In this unfuelled discharge ( $I_p=1.7\text{MA}/B_t=2.7\text{T}$ ,  $q_{95}=5$ ,  $P_{\text{NBI}}=17.5\text{MW}$ ), the temperature ELM collapse affects a large part of the plasma core, whereas the density collapse does not extend further than  $r/a\sim 0.8$ . This large ELM affected area compared to the baseline plasma in figure 5 is not caused by the difference in  $q_{95}$  between the discharges [12], however a difference in the core magnetic shear may play a role. It has been found that this ELM affected area of the temperature collapse can be greatly reduced by deuterium fuelling [5]. Figure 6 shows that fuelling an otherwise similar discharge with deuterium ( $10^{22}$  electrons/second) indeed strongly mitigates the effect of the temperature collapse. The effect of the density collapse on the other hand has been reduced by a much lesser extent, as a result of which the ELM losses have been turned from being dominated by conductive losses in the unfuelled case to a more even distribution of conductive and convective losses in the fuelled discharge. This however is accompanied by a reduction in pedestal confinement in this case as both  $T_{e,\text{ped}}$  and  $n_{e,\text{ped}}$  are reduced (Figure 6).

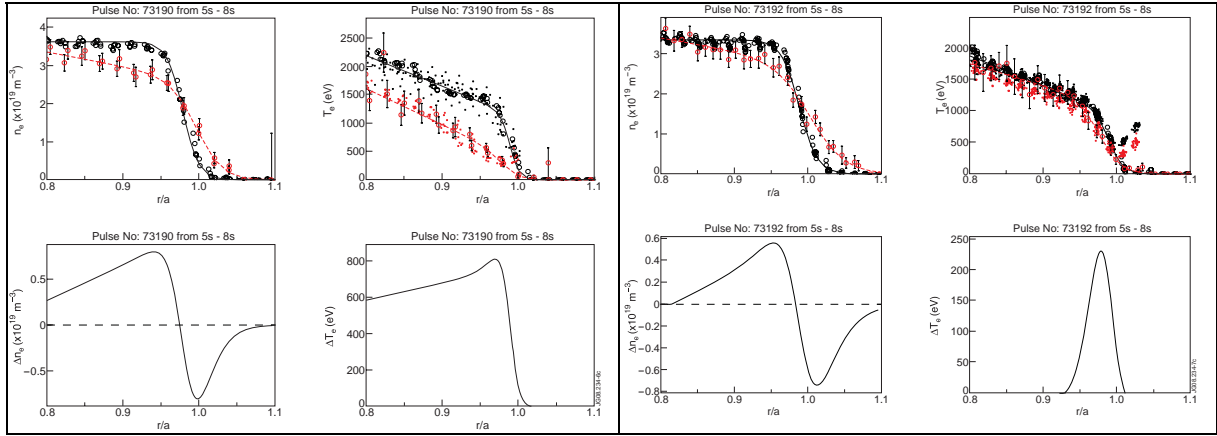


Figure 6: Pre-ELM (black) and Post-ELM (red) Density and Temperature profiles from HRTS and their difference in an (a) unfuelled AT plasma and (b) a similar plasma with  $10^{22}$  electrons/second deuterium fuelling. ( $I_p=1.7\text{MA}/B_t=2.7\text{T}$ ,  $q_{95}=5$ ,  $P_{\text{NBI}}=17.5\text{MW}$ ). The small symbols are ECE  $T_e$  data for comparison.

## 6 Convective and conductive ELM losses

The electron ELM losses can be calculated from the convective and conductive losses in Figures 5 and 6. If it is assumed, as in [13], that the ELM losses are poloidally symmetric and that  $\Delta T_i = \Delta T_e$  and  $T_i = T_e$  then the total ELM energy loss is ( $T_e$  and  $n_e$  are pre-ELM profiles):

$$\Delta W_{\text{ELM}} \approx 3 \cdot k \cdot \left( \int \Delta T_e \cdot n_e \cdot dV + \int T_e \cdot \Delta n_e \cdot dV \right) \quad (1)$$

With the first part being the conductive ELM losses and the second part the convective losses. The integration takes place over the confined plasma volume. To verify that this method works with the JET data the sum of the convective and conductive losses have been compared to the ELM energy losses estimated from the diamagnetic energy measurement in figure 7. There is generally a good agreement between the two measurements with the kinetic estimate  $\sim 15\%$  higher than the diamagnetic estimate. The spread in the data is only partly due to statistical noise in the HRTS measurements. As can be seen in Figure 3, there is a large natural spread in pedestal  $T_e$ ,  $n_e$  and  $\Delta W_{\text{ELM}}$ , even though this discharge has very regular type I ELMs. This spread is partly caused by variations in the plasma parameters in the selected time window but is also characteristic for type I ELMs; the ELM trigger does not always occur at exactly the same level of pedestal  $T_e$ ,  $n_e$  or stored energy [12].

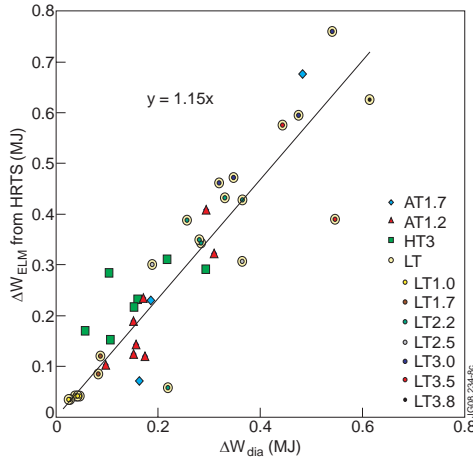


Figure 7: kinetic ELM losses from HRTS measurements versus diamagnetic ELM energy losses measurements. The drawn line is a linear fit to the data showing that  $\Delta W_{ELM} = 1.15 \times \Delta W_{dia}$ .

The convective and conductive ELM losses for the low and high triangularity baseline plasmas combined are compared to pedestal electron collisionality  $\nu_e^*$  in Figure 8a. The trends as found in [11,12], i.e. decreasing ELM losses with increasing  $\nu_e^*$  are confirmed by these data. However, as convective and conductive losses are independently determined from the HRTS profiles their ratio can now be quantified. The convective losses do not vary significantly and are  $\sim 5\%$  of  $W_{ped}$  over a large range of  $\nu_e^* < 0.1$  to  $\nu_e^* > 0.5$  whereas the conductive losses, be it that the scatter is large, strongly decrease from  $\sim 20\%$  of  $W_{ped}$  to  $5\%$  of  $W_{ped}$  with increasing  $\nu_e^*$ . Note that the low triangularity data cover a large range of current from 1MA-3.8MA. The high triangularity discharges selected for this analysis reside at  $\nu_e^* \sim 0.5$  with  $\Delta W_{cond} \sim \Delta W_{conv} \sim 5\%$ , as the pedestal  $n_e$  is high and  $T_e$  is low (Figure 1).

This trend is not repeated for the AT plasmas in Figure 8b. Still a large spread in conductive losses from  $< 5\%$  to  $\sim 25\%$  of  $W_{ped}$  is found, but  $\nu_e^*$  remains unvaried at  $\sim 0.1$ . This should be compared with the data in Figure 6. The two plasma presented there have  $\nu_e^* \sim 0.1$  whereas a large reduction in conductive losses can be obtained by  $D_2$ -gas fuelling. The gas fuelling leads to a reduction in  $T_e$  and  $n_e$  (Figure 6). Note that in the case of AT plasmas the reduction of the conductive ELM losses also leads to a much smaller ELM affected area. This has not been observed for the baseline plasmas. A systematic study with a more fine  $D_2$  gas fuelling scan in AT plasmas [5] showed a similar result. Here small levels of gas fuelling lead to an increase of X-point radiated power and hence in a cooling of the pedestal leading to smaller ELMs, and reduced ELM energy losses and ELM affected area. This should be a topic of further study, as the different ELM energy loss characteristics of AT and baseline plasmas may give new information towards the understanding of the mechanisms that determine the ELM energy losses.

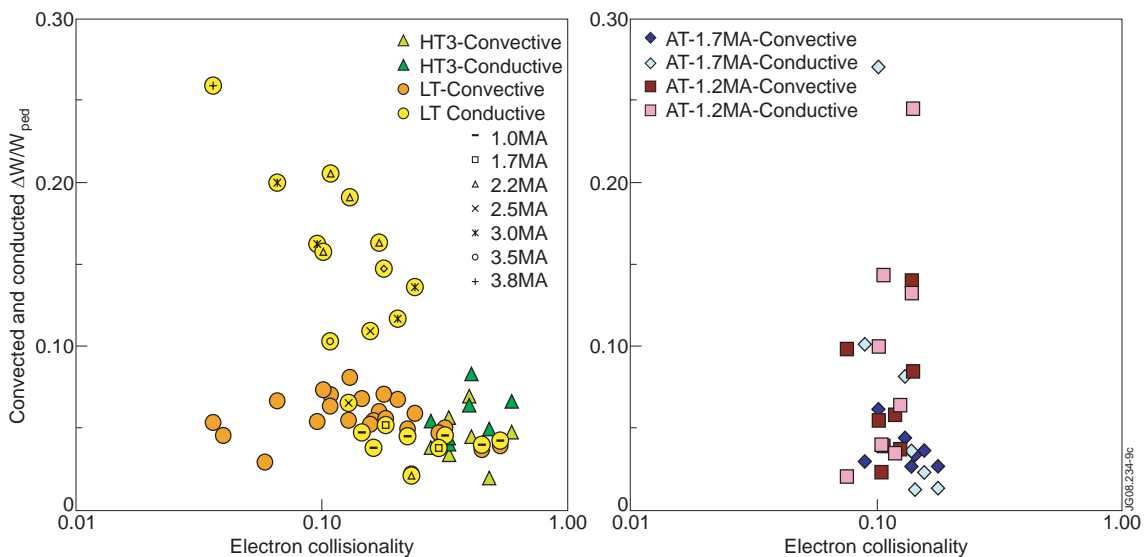


Figure 8: Fractional Convective and conductive ELM energy losses versus electron collisionality  $\nu_e^*$  for (a) the baseline plasmas and (b) the AT scenarios

## 7 Summary and Conclusions

New diagnostic capability on JET has opened the way for research toward deeper understanding of the pedestal structure and pedestal dynamics on JET. In this paper the new High Resolution Thomson Scattering system has been exploited to investigate the conductive and convective ELM losses and the pedestal dynamics for a large range of plasma parameters and plasma conditions. The dynamics of the density pedestal profile on JET as measured with HRTS is very similar to that observed with reflectometry measurements on DIII-D [8], AUG [9] and JT-60 [10]. The density deposited in the SOL after an ELM collapse is diffused on a transport time scale parallel to the magnetic field line toward the divertor. On a faster time scale plasma filaments have been observed in the SOL  $<100\mu\text{s}$  after an ELM collapse. It has been estimated that these filaments can carry up to 30% of the energy loss caused by the ELM collapse. As only a fraction of the ELM energy loss is distributed over the main chamber wall by the filaments [17], most of the energy will be deposited on the divertor target. In this paper the separate conductive and convective ELM losses are characterised. It is to be expected that the particle transport losses lead to a lower power load on the target than an equivalent amount of energy loss due to heat losses. This follows from the observation that the parallel transport of the convective losses is at least an order of magnitude slower than that of the conductive losses [18]. It is therefore beneficial to operate in a regime with dominating particle losses. However, the convective loss fraction of  $W_{\text{ped}}$  remains rather unchanged for a wide range of plasma parameters as has also been observed in [10-13,15]. The difference in dependence on collisionality of the conductive losses between the baseline and AT plasmas needs to be further studied as it may give deeper understanding of the physics of the ELM dynamics.

## Acknowledgements

This work was funded jointly by the UK Engineering and Physical Sciences Research Council and by the European Communities under the contract of Association between EURATOM and UKAEA. It was carried out within the framework of the European Fusion Development Agreement. The views and opinions expressed herein do not necessarily reflect those of the European Commission.

## References

- [1] Pitts R.A. et al 2007 P 49th APS Division of Plasma Physics Meeting (Orlando, FL, USA)
- [2] Y Sarazin et al. Plasma Phys. Control. Fusion, 44 (2002) 2445
- [3] M. Becoulet, Plasma Phys. Control. Fusion, 45 A93
- [4] Rimini F.G. et al Nucl. Fusion 45 (2005) 1481
- [5] M.N.A. Beurskens et al. Nucl. Fusion 48 (2008) 095004
- [6] M.Jakubowski et al, submitted to J.Nucl.Mater
- [7] A. Kirk et al. Journal of Physics : conf Series 123 (2008) 012011
- [8] L Zeng et al, Plasma Phys. Control. Fusion 46 (2004) A121–A129
- [9] I. Nunes et al, Nucl. Fusion 45 (2005) 1550-1556
- [10] N. Oyama, Nucl. Fusion 44 (2004) 582–592
- [11] A. Loarte et al, Plasma Phys. Control. Fusion 44 (2002) 1815-1844
- [12] A. Loarte et al, Physics of plasmas 11-5 (2004), 2668-2678
- [13] A.W. Leonard et al, J. Nucl Mat. 313-316 (2003) 768-776
- [14] G. Saibene, Nucl. Fusion 45 (2005) 297
- [15] A.Kirk et al, Plasma Phys. Control. Fusion 49 (2007)
- [16] Pasqualotto R. et al 2004 Rev. Sci. Instrum. 75 3891
- [17] W Fundamenski This conference.
- [18] R.A. Pitts, submitted to J.Nucl.Mater